Journal of Modern Optics

ISSN: 0950-0340 (Print) 1362-3044 (Online) Journal homepage: http://www.tandfonline.com/loi/tmop20

Surface Profiling by Analysis of White-light Interferograms in the Spatial Frequency Domain

Peter de Groot & Leslie Deck

To cite this article: Peter de Groot & Leslie Deck (1995) Surface Profiling by Analysis of White-light Interferograms in the Spatial Frequency Domain, Journal of Modern Optics, 42:2, 389-401, DOI: 10.1080/09500349514550341

To link to this article: https://doi.org/10.1080/09500349514550341

JOURNAL OF MODERN OPTICS, 1995, VOL. 42, NO. 2, 389–401

Surface profiling by analysis of white-light interferograms in the spatial frequency domain

PETER DE GROOT and LESLIE DECK
Zygo Corporation, Laurel Brook Road, Middlefield, CT 06455, USA

(*Received 25 January 1994; revision received 8 May 1994 and accepted 28 June 1994*)

Abstract. We describe a scanning white-light interferometer for high-precision surface structure analysis. Interferograms for each of the image points in the field of view of the instrument are generated simultaneously by scanning the object in a direction perpendicular to the object surface, while recording detector data in digital memory. These interferograms are then transformed into the spatial frequency domain and the surface height for each point is obtained by examination of the complex phase as a function of frequency. The final step is the creation of a complete three-dimensional image constructed from the height data and corresponding image plane coordinates. The measurement repeatability is better than 0·5 nm r.m.s. for a surface height range of 100 μm.

1. Introduction

Perhaps the most remarkable thing about a white-light interference pattern is that it is very difficult to obtain. Fringes only appear in a limited spatial region, and may not appear at all if the interferometer is not perfectly focused and balanced for dispersion. On the other hand, the localization of white-light fringes can be used to advantage in interferometric profilers, since it effectively eliminates the phase ambiguity problem. With conventional laser-based interferometers, discontinuous height variations or surface roughness can result in interferometric phase ambiguities that are difficult or impossible to interpret. For this reason, new forms of innovative surface profilers have been proposed that are specifically designed to function with white-light [1].

Generally these white-light surface profilers base their measurement principle on the common observation that white-light fringes are hard to get. In other words, they use fringe contrast to identify surface height. One way to do this is to mechanically modulate the optical path difference (OPD) of an imaging interferometer such as an interferometric microscope, and record the position of peak fringe contrast for each point in the field of view as a function of OPD. The result is a map of surface height.

This paper takes a different point of view. A white-light interferogram may be considered to be a sum of a number of independent fringe patterns of various colours that are added together by incoherent superposition. Fourier analysis of the interferogram can recover these virtual single-colour fringe patterns in order to determine their relative strengths and phases as a function of wavenumber. It is then possible to precisely measure distances by observing how the phases vary as a function of wavenumber. These physical principles, so well understood and widely

applied in the spectroscopic analysis of one-dimensional interferograms, are exploited in our research to generate three dimensional imaging of surfaces with white light. For us, white light is not just a source of highly-localized fringes, it is a rich repository of multiple wavelengths which identify surface features with extraordinary accuracy.

2. Mapping surfaces with white light fringes

The use of white light in interferometry has a long history. Already in 1665, Hooke noted that the colours seen in white-light interference patterns are a sensitive measure of thickness between reflecting surfaces [2]. In 1893, Michelson used white light to estimate the size of a series of step-shaped etalons as part of the procedure leading to the first comparison of the wavelength of light with the International Prototype Meter [3]. Many of the traditional optical instruments for calibrating gauge blocks employing white light or multiple-colour sources, as well as special microscopes suitable for white-light interferometry, have been in use for a number of years [4]. White-light interference microscopes have been widely used for measuring film thicknesses and monitoring surfaces with discontinuities several wavelengths deep.

Although the basic principles of white-light and multiple-colour interferometry are fundamental concepts of optics, the practical implementation of these principles in automated instruments is a comparatively recent development. A detailed description of an automated white-light thickness gauge for plane-parallel films appeared in an article by Flournoy *et al.* in 1972 [5]. This instrument is capable of measuring thicknesses from 2·5 to 500 μm with a resolution of 0·05 μm using mechanically-scanned interferometer mirrors and electronic intensity detection. Another white-light interferometer introduced by Youngquist *et al.* is designed to determine positions and magnitudes of reflection sites within miniature optical assemblies [6]. Hitzenberger [7] and Fercher *et al.* [8] have extended broadband interferometry to diagnostic measurements of the eye. Recent work by Huang *et al.* with biological samples has resulted in a new and promising form of medical imaging called coherence domain reflectometry [9].

Relatively few methods for obtaining full three-dimensional representations of surface topography with white-light interferometry have been reported. The methods described in the literature are almost exclusively based on the analysis of fringe contrast. Briefly described, the physical principles underlying the fringe-contrast method for topographical measurement are as follows. A typical white-light interferogram can be approximated by an overall constant I_0 and a series of sinusoidal interference fringes modulated by an envelope function:

$$I = I_0[1 + V\cos\phi]. \tag{1}$$

The envelope function V is the fringe contrast, which varies much more slowly with OPD than the fringe phase ϕ. The fringe contrast has many synonyms, such as fringe visibility, modulation, signal variance, modulus of the complex degree of coherence, and so on, depending on the context. A basic principle of optics is that the peak contrast for white-light fringes in an ideal, dispersion-compensated interferometer occurs when the OPD is zero. Thus, one way to measure surface topography is the determination of the position of maximum contrast simultaneously for an array of image points, using an interferometer equipped with mechanical means for varying the OPD.

One of the first practical systems for automated, three-dimensional measurements of surface topography using white-light interferometry is described by Balasubramanian [10]. The method involves scanning either the reference mirror or the object in discrete steps, measuring the fringe contrast for each pixel at each scan position, and in this way determining for each surface point the position of maximum fringe contrast. The scan position for which the contrast is maximum is a measure of the relative height of a particular surface point. An important feature introduced by Balasubramanian relates to the efficient use of computer memory. At each point in the scan, the current fringe contrast for each pixel is compared to a stored value, and if it is larger, it replaces the stored value for that pixel, together with the current scan position. If the current fringe contrast is less than the stored value, it is discarded.

White-light interferometric microscopes are particularly useful for sectioning images according to surface height, in a manner analogous to confocal microscopes, but without the complexity and high cost of confocal instruments. Davidson has applied automated mechanical scanning and detection of peak fringe contrast to the profiling of microscopic objects such as integrated circuits [11]. The Davidson apparatus is based on a common Linnik interference microscope, with the addition of electronic means for processing of video images to obtain fringe contrast information, and a PZT-actuated object stage controlled by a computer. Similarly, Lee and Strand have shown that white-light interfereometry can improve lateral resolution over conventional microscopes, in addition to providing information about surface topography [12].

There have been many improvements related to rapid determination of fringe contrast in white-light interferometers, and to the reduction of data to representations of three-dimensional images. Dresel *et al.* have constructed a white-light interferometer that uses a mechanical translation stage to scan the object [13]. For each scan position, intensities for three different interference phases are obtained by small displacements of a reference mirror. These intensities are used in a simple formula to calculate the fringe contrast for each image pixel. By recording the position of maximum fringe contrast over the total range of the translation stage, Dresel *et al.* have obtained several remarkable graphical images of three-dimensional objects, including those considered very rough according to the standards of conventional interferometry.

Another way of rapidly measuring fringe contrast is to digitally filter the interference data. Chim and Kino have introduced two different digital filter algorithms for rapidly extracting the fringe contrast envelope, one based on Fourier transforms and the other based on the Hilbert transition [14, 15]. Caber has adapted digital filter concepts from communications theory to recover fringe contrast envelopes [16].

Modern electronic and computational means for rapidly determining fringe contrast have dramatically increased the range of applications of white-light interfereometry. However, using the position of maximum fringe contrast for mapping surface features has many fundamental disadvantages. The contrast method requires a great number of calculations, but most of the results are discarded, and very few or only one data point per pixel is preserved for the final measurement. Thus the method does not make effective use of all of the available interference data. In particular, the method can be extremely sensitive to random noise, such as spikes or missing data points, that would be interpreted as positions of high fringe contrast.

Another problem is that most fringe contrast calculations are highly wavelength dependent, and may fail if the mean wavelength or other spectral properties of the source vary because of changes in environmental conditions or adjustments in illumination strength. Also, the fringe contrast envelope often must be assumed to be of a particular functional form, such as Gaussian, in order to be accurate; and distortions of this envelope shape due to surface colours or unexpected or unusual source spectra can also lead to significant errors.

3. Analysis in the spatial frequency domain

The limitations of the fringe-contrast method are nowhere more acutely felt than in the study of optical waveguides and fibres. First-order waveguide and material dispersion shifts the position of peak fringe contrast with respect to the zero OPD position, and higher-order dispersion can strongly distort the fringe contrast envelope. These effects can dramatically reduce the accuracy of white-light interferometric methods of distance measurement, and have encouraged the study of alternative approaches to the simple detection of fringe contrast.

One such alternative is to analyse interferograms for their spatial frequency content, using Fourier transform methods. By transforming interference data to the spatial frequency domain, it is much easier to extract optical lengths and dispersion parameters in the study of solid-state waveguides and optical fibres. For example, Kohlhass *et al.* have developed a Fourier-transform method for correcting dispersion-corrupted interferograms from integrated-optical waveguides [17]. Similarly, Danielson and Boisrobert have described a fibre-optic instrument evaluated as part of a program to develop diagnostic probes for testing the guiding characteristics of semiconductor laser sources [18]. These authors make a convincing argument that if there is a large amount of dispersion, processing is best performed in the spatial frequency domain, where the phase angle as a function of wavenumber can be explicitly calculated.

The principles of frequency-domain analysis do not appear to have been applied to the realization of three-dimensional representations of surface topography with white light. This is perhaps due to the absence of a compelling application, such as three-dimensional depth profiling of a dispersive material, where the fringe-contrast method would obviously be inadequate. However, as the following mathematical development will show, some of the advantages of frequency domain analysis are worth looking into even for less challenging problems.

When a single-colour (monochromatic) source illuminates a two-beam interferometer equipped with a square-law intensity detector, a pattern is generated in space that appears as a sequence of sinusoidal fringes of spatial frequency k and phase ϕ. By spatial frequency we mean the rate of change of phase, in radians, as a function of mechanical displacement of the reference mirror of the interferometer. This quantity k is also known as the angular wavenumber, or simply the wavenumber, of the source light. The relationship between the wavenumber, the phase, and an OPD Z in the interferometer is given by

$$\phi = kZ. \tag{2}$$

The OPD Z is also a function of wavenumber, unless the interferometer is perfectly compensated for dispersion [19].

Now consider the general case, a polychromatic or white-light source. There are a series of wavenumbers present, each resulting in a separate interferogram that adds

incoherently to the others to produce the final white-light fringes. The relative phase of each of these interferograms can be expressed in terms of a Taylor series expansion about a mean wavenumber k_0:

$$\phi = \phi_0 + (k - k_0)\left.\frac{\mathrm{d}\phi}{\mathrm{d}k}\right|_{k_0} + \frac{(k - k_0)^2}{2}\left.\frac{\mathrm{d}^2\phi}{\mathrm{d}k^2}\right|_{k_0} + \ldots . \tag{3}$$

The first, constant term ϕ_0 is the phase for $k = k_0$ and is given by

$$\phi_0 = k_0 Z_0. \tag{4}$$

The second term, which is the first-order variation of phase with wavenumber, can be written

$$\left.\frac{\mathrm{d}\phi}{\mathrm{d}k}\right|_{k_0} = Z_0 + k\left.\frac{\mathrm{d}Z}{\mathrm{d}k}\right|_{k_0} = G_0. \tag{5}$$

The distance G_0 is the group velocity OPD for $k = k_0$, and it is equal to the so-called phase velocity OPD Z_0 only for the special case of an interferometer that has been perfectly compensated for dispersion. The phase as a function of wavenumber can now be written

$$\phi = k_0 Z_0 + (k - k_0)G_0 + \frac{(k - k_0)^2}{2}\left.\frac{\mathrm{d}G}{\mathrm{d}k}\right|_{k_0} + \ldots . \tag{6}$$

Equation (6) shows that if the phase as a function of wavenumber is known in the neighbourhood of the mean wavenumber k_0, then it is possible to recover the phase velocity OPD Z_0, the group velocity OPD G_0, the rate of change $\mathrm{d}G/\mathrm{d}k$ of the group velocity OPD with wavenumber, and other terms of higher order, depending on the quality of the data. In other words, there is a terrific amount of information in the frequency-domain description of an interference pattern [20].

What is needed then is a series of interference phase values for a series of wavenumbers. This information may be extracted from an interference function $I(Z)$ through the normalized Fourier transform

$$P(k) = \int_{-\infty}^{\infty} I(Z)\exp(-\mathrm{i}kZ)\,\mathrm{d}Z. \tag{7}$$

The desired phase evolutions is then given by

$$\phi(k) = \tan^{-1}(\mathrm{Im}\{P(k)\}/\mathrm{Re}\{P(k)\}). \tag{8}$$

The problem of how to measure surface topography without relying on fringe contrast is now solved, at least in principle. A mechanical scan of an imaging interferometer over a range of OPD values results in a digital representation of the interference function for each image point in the field of view of the instrument. The Fourier transform of each individual interferogram results in a sequence of phase values that can be used to determine the local surface height. The analysis takes place entirely in the spatial frequency domain, and the fringe contrast is never calculated.

4. The interferometer

The instrument we have used in our research is based on the amplitude-division interferometer shown in highly simplified form in figure 1. An incandescent lamp illuminates an interferometric microscope objective via a beam-splitter prism. The

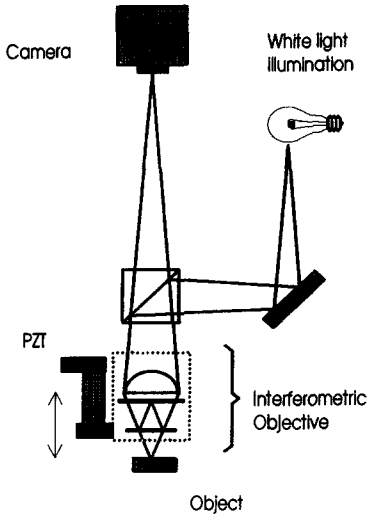

Figure 1. Simplified drawing of the interferometric microscope used in the experiments.

Mireau-type objective shown in the figure has a beam-splitting element that transmits one portion of the beam to a reference mirror and the other beam to the object. The two beams reflected from object and reference are recombined and projected onto a charge-coupled device (CCD) video camera, which generates a signal proportional to the resultant beam intensity produced by the interference effect.

The objective lens focuses the image of the object surface onto the sensing element of the camera, so that each pixel in the digital image corresponds to a point or small region of surface. When the objective is properly adjusted, an interference pattern is observed by the camera even for the extended (spatially incoherent) illumination produced by the incandescent source.

The objective is held in place by a commercial piezo-electric fixture that is capable of precise vertical scans, which has the effect of varying the OPD of the interferometer. A sequence of intensity data frames are acquired by the camera and stored in microcomputer memory during a continuous scan of the objective lens. The stored data consists of an array of interferograms, one for each pixel, representing the variation in intensity as a function of scan position. For example, if the camera resolution is 256×256, and if 64 images are stored during the scan, then there will be approximately 64 000 interferograms, each 64 data points in length. A computer-simulated white-light interferogram, sampled at the rate of one frame every 125 nm (round-trip OPD) and corrupted by a random intensity noise, is shown in figure 2.

For some objects of interest, a long scan length of several tens of microns is required to accommodate all of the surface features. The computer memory requirements would soon become oppressive if we needed to store all of the data for these long scans. However, since good white-light fringes appear only over a small portion of the scan, most of the raw intensity data can be discarded. We use a simple frequency-based discriminator sensitive to variations in the data to determine, for each pixel, the position of interference and a circular buffer scheme to store sufficient data symmetrically disposed about the interference peak [21, 22]. In this way,

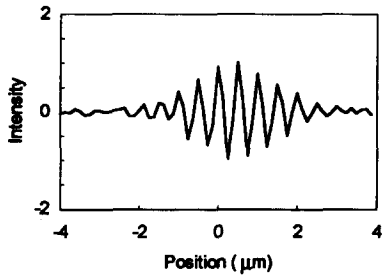

Figure 2. Graph depicting a typical interferogram for one pixel in the detector array.

acquisition is rapid and the total number of points stored, and required processing, remains fixed for all scan lengths.

After the data has been acquired, the computer analyses each of the stored interferograms to discover its composition in terms of wavenumbers and corresponding phrases. Starting with a single-column array of N intensity values I_i taken at equally-spaced OPD positions Z_i, the contribution to the interferogram for a particular wavenumber k_j is found by the discrete Fourier transform

$$P_j = \sum_i I_i \exp(-ik_j Z_i). \tag{9}$$

The result P_j is the jth component of the Fourier transform. The complex quantity P_j can be expressed as

$$P_j = |P_j| \exp(i\phi_j). \tag{10}$$

The transformed interferograms now represent, for each pixel, the relative strength $|P_j|$ and interferometric phase ϕ_j as a function of wavenumber k_j. In figure 3 a graph is shown of the relative strength $|P_j|$ as a function of the wavenumber k_j, resulting from the Fourier transform of the interferogram shown in figure 2. The phase ϕ_j as a function of the wavenumber k_j for this example is shown in figure 4. It is important to note that the Fourier transform will be effective only if a significant portion of the white-light interferogram is represented in the data set. If the data set is too narrow, the sampling window will be convolved into the calculation and may distort the phases.

Most of the useful information in the Fourier transformed data is contained in the region where the relative strengths $|P_j|$ are large. A simple peak-finding search is performed to locate this region. Alternatively, if the scan rate and the spectral characteristics of the source are precisely known, the location of this region can be predicted. For example, a source having a mean emission wavelength of 500 nm will have a peak at wavenumber $k_0 = 2\pi/500$ nm. If the interferogram has 64 data points acquired at round-trip OPD intervals of exactly 125 nm, then wavenumber k_0 is equivalent to 16 cycles per 64-point scan. The predicted peak for the example in figure 3 is indicated by an arrow.

Once the region of interest in the Fourier transformed data is identified, either by prediction or by automatic search, a series of pairs (ϕ_j, k_j) are collected from this region for use in calculating the parameters in equation (6). The modulo 2π

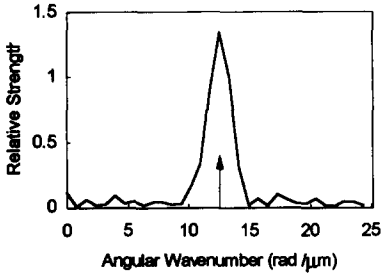

Figure 3. Graph of the relative strengths of the various spatial frequency components of the interferogram shown in figure 2.

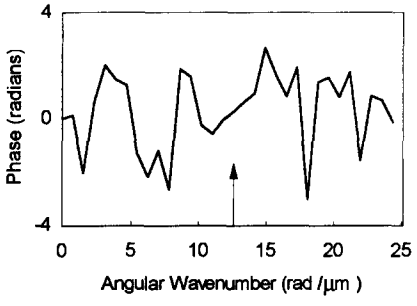

Figure 4. Graph of the interferometric phases corresponding to the various spatial frequencies shown in figure 3. The arrow indicates the phase for the dominant spatial frequency of the interferogram.

ambiguities in the phase data are removed by recursive application of the following formula:

$$\phi_j = \phi_j - 2\pi \,\mathrm{Int}\,\{(\phi_j - \phi_{j\pm 1})/2\pi\}. \tag{11}$$

The $\pm$ relates to whether the recursion is in the direction of increasing or decreasing values of j. The function Int { } returns the nearest integer to its argument and is used to force continuity between adjacent phase values.

Next, a polynomial is fitted to the (ϕ_j, k_j) data pairs in order to estimate the terms appearing in equation (6). A linear least-squares fit is generally sufficient, unless a large amount of second-order dispersion is present in the interferogram, in which case a quadratic fit is sometimes appropriate. For the purpose of measuring surface topography, the slope and constant terms are of primary interest. In particular, the group velocity OPD can be readily calculated from the phase slope and an inverted form of equation (5):

$$G_0 = \left.\frac{\mathrm{d}\phi}{\mathrm{d}k}\right|_{k_0}. \tag{12}$$

The relationship between the group velocity OPD and the actual physical topography of a surface is governed by the group velocity index n_G. Referring again to figure 1, a relative change ΔG in round-trip group velocity OPD corresponds to a change Δh in physical surface height according to

$$\Delta h = \frac{\Delta G}{2n_G}. \tag{13}$$

This calculation is performed for each pixel in the image, resulting in a three-dimensional map $\Delta h(x, y)$ of the surface topography, where x, y are the surface coordinates.

An optional next step in the data processing consists of improving the resolution of the measurement for each pixel by making use of the constant term $k_0 z_0$ appearing in equation (6). The constant term is obtained automatically as a consequence of the least-squares fit performed in the previous step, but its value is only known modulo 2π. This difficulty is avoided in the following calculation, which makes use of the approximate Δh value calculated from the phase slope:

$$\Delta h' = \frac{1}{2n}\left[\frac{(\phi_0 - \alpha)}{k_0} - \frac{2\pi}{k_0}\,\mathrm{Int}\left\{\frac{(\phi_0 - \alpha) - (2k_0 \Delta h n)}{2\pi}\right\}\right]. \tag{14}$$

The quantity n is the index of refraction, sometimes referred to as the phase velocity index of refraction, to distinguish it from n_G. The constant phase offset α is due to factors such as spatial coherence phenomena and phase-change on reflection. It represents an overall piston term to the topography and can therefore be subtracted out without corrupting the topographical features. Generally, the quantities n, n_G and α are all material dependent and must be known for the measurement to be accurate. For many objects, however, it is sufficient to let $n = n_G = 1$ and assume that α is uniform over the field of view.

Equation (14) provides essentially the same measurement resolution as conventional phase-shifting interferometry [23], without the problem of phase ambiguity. The final step in the signal processing is the construction of a representation of the surface topography using the results $\Delta h(x, y)$ or $\Delta h'(x, y)$ for each pixel.

Spatial frequency domain analysis has the useful characteristic that the data sampling interval Z_i can be almost anything. Even data sampled at less than the Nyquist frequency (two data points per fringe) is useful [24], provided that care is taken to avoid segmenting and overlapping the frequency bandwidth [25]. For example, if data is acquired at phase intervals of $5\pi/2$ the mean frequency k_0' of the under sampled data is five times lower than that of the actual interference pattern, but the bandwidth Δk and the rate of change $\mathrm{d}\phi/\mathrm{d}k$ are the same. The phase ϕ_0' at k_0' is also the same as the phase ϕ_0.

Finally, we present in figures 5 and 6 the results of two examples of isometric three-dimensional plots obtained with the instrument using a phase interval of $\pi/2$. These two figures are good examples of measurements that are generally not possible to make with interferometers equipped with monochromatic sources.

5. System performance

We have performed a number of experiments to evaluate the effectiveness of surface profiling by frequency-domain analysis (FDA) of white-light interferograms. All of these tests were performed with an ordinary halogen light source for microscope illumination.

First, we compared FDA directly with widely known fringe contrast algorithms, such as those cited in section 2, using identical raw data sets. The most accurate fringe contrast methods involve a least-squares fit of a Gaussian, parabolic or sinc-function envelope to a range of contrast values. In general, the performance of the best fringe contrast methods, in terms of repeatability on smooth, flat parts, is

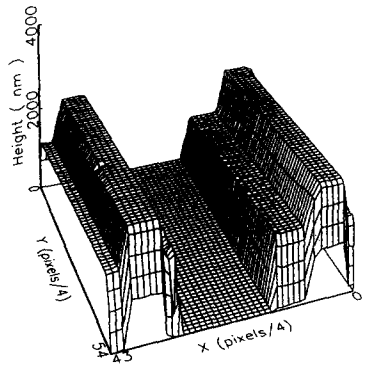

Figure 5. Three-dimensional image obtained with the experimental system, using a 2·5 × objective. This is the surface-height plot of the sensing head for a magnetic-storage hard disk drive. The surface of this object has large discontinuities that can confuse conventional laser-based interferometers. The original 256 × 256 image has been compressed by a factor of four to make the graph more readable.

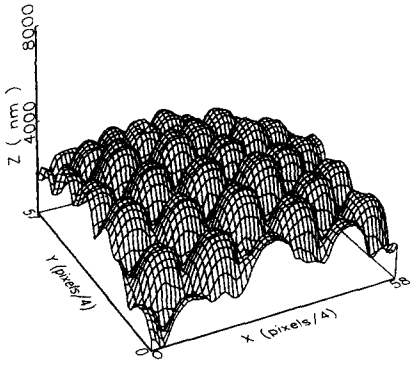

Figure 6. Surface-height plot of a moth's eye, as seen with a 50 × objective in the experimental system. The large surface variations are easily accommodated with the white light interferometer and frequency domain analysis.

the same as that of the phase-slope measurement (equation (13)), provided that we include the same number of data points (64) in the least-squares fit to the envelope. A typical single-measurement repeatability is 3 nm r.m.s. for both techniques. However, since fringe contrast methods commonly use only a few data points near the peak of the envelope, a more realistic value would be greater than 3 nm. The repeatability is determined by subtracting successive surface height measurements on a silicon carbide sample and calculating the r.m.s. residuals over the field of view.

Next comes the question of high-resolution measurements that make use of the constant term $k_0 z_0$ (equation (14)). An equivalent measurement based on fringe contrast requires a second calculation of the mean phase of the interference fringes. The repeatability of this second calculation depends of course on the particular algorithm chosen. Using the familiar five-bucket Schwider-Hariharan algorithm [26] we were able to achieve repeatabilities of 0·7 nm, compared to 0·4 nm for FDA with the identical raw data set. The difference is related to the number of processed

data points. Improved repeatability may be possible with more complicated phase-calculation algorithms; however, FDA provides all the necessary phase information without separate data-processing. We view this as a significant advantage of FDA.

In another experiment, we tested the ability of FDA to compensate for variations in the spectral distribution of the source. We installed an ND2 filter after the source, and then increased the source current to compensate for the lost light intensity. The mean wavelength decreased by 3·8% from 583 to 561 nm, which, for conventional methods of scanning white-light interferometry, would result in calibration errors of the same relative magnitude. However, since FDA provides detailed spectral information, including the mean effective wavelength for every pixel in the field of view, the net calibration error was less than 0·1%. Here again, it may be possible to include a separate calculation to conventional fringe contrast algorithms to achieve substantially the same result, but only at the price of additional data processing.

Several experiments have confirmed the increased flexibility of FDA with regard to the data sampling interval. Fringe contrast methods rely on a discrete contrast calculation in the neighbourhood of each data point in the interferogram. Typically, this calculation is specific to a specific data sampling rate, such as $\pi/2$. Deviations from this interval can severely distort the calculated contrast envelope. Since FDA does not require any specific data sampling interval, we are able to alter the interval over a considerable range without changing the basic algorithms. For example, an adjustment of the data interval from $\pi/2$ to $2\pi/3$ increases the data acquisition speed by 30% while maintaining the measurement repeatability below 1 nm. The extreme case of sub-Nyquist sampling has been discussed in a prior publication [24].

We have also compared our results with the literature. Many of the first white-light profilometers were designed for rather coarse vertical resolution, on the order of 1 μm [13]. Several researchers using microscopes have now reported a vertical resolution of less than ten nanometers (see, for example, Sandoz and Tribillon [27], Montgomery and Fillard [28]). The best reported results to date for three-dimensional profiling by fringe contrast are those of Caber *et al.* [29]. Using a digital low-pass filter and envelope fitting. Caber claims a surface-height resolution of 2 nm, which, allowing for possible differences in hardware and in the definitions of resolution and repeatability, is close to our experience. For improved resolution, Caber proposes a two-step procedure, involving a preliminary white-light measurement followed by conventional phase-shift interferometry (PSI) with a narrow-band filter. The two separate measurements may then be combined in software, resulting in a claimed resolution of 0·3 nm. This is better than we are able to achieve in our laboratory experiments, but is of comparable magnitude. The two-step technique has the advantage that the PSI measurement may be repeated rapidly for data averaging. However, it is not always reliable to work with independent data sets when resolving fringe ambiguities, and PSI measurements suffer from a limited depth of focus. The choice of measurement technique may eventually depend on the specific application.

The issue of measurement speed is especially ticklish, since so much depends on the particular implementation, software optimization and computing platform. Caber uses custom digital signal processing hardware to achieve a vertical scan rate of 0·5 $\mu m\,s^{-1}$ with a claimed repeatability of 2 nm [16]. We acquire data at 2 $\mu m\,s^{-1}$ using conventional microcomputer hardware and generate a profile repeatable to 0·4 nm. The difference in speed is largely due to our data acquisition algorithm,

which stores only the most meaningful portion of the interferograms, vastly reducing the number of computations required during the vertical scan. The improved repeatability for comparable measurement times is a benefit of FDA, which does not require a separate PSI measurement for improved accuracy.

A few words related to the influence of noise are in order. A comparative quantitative study of FDA in the presence of noise is beyond the scope of this paper; but it is possible to make a few qualitative remarks based on experience. Generally, FDA and fringe contrast methods are expected to have similar sensitivity to vibration and intensity noise, provided that the fringe contrast algorithm processes as many raw data points, and is accomplished by a PSI calculation to improve precision. The pre-transformed data set in our experiments is 64 points large for each pixel. In practice, fringe contrast methods rarely use this many points in the final fitting routines that determine the peak of the envelope, and PSI algorithms typically use three to five points, not 64. In our experience, we have never encountered a case where the fringe contrast method outperformed FDA.

6. Conclusions

Whenever the issue of how to improve scanning white-light interferometers is raised, we inevitably are drawn to some form of phase or frequency analysis such as PSI to complement the well-known fringe contrast methods. In this paper we have taken the viewpoint that the entire data processing should take place in the spatial-frequency domain. Although this is not a revolutionary concept in optics, it is a divergence from current trends in three-dimensional surface profiling.

These experiments demonstrate that processing white-light interferograms in the frequency domain have significant advantages for three-dimensional profiling and surface structure analysis. The excellent measurement repeatability and high speed set the present work apart from the more familiar fringe contrast methods. Further benefits include the ability to handle more complex measurement problems that may arise due to variations in the emission spectrum of the source, distortions of the fringe contrast envelope, and changes in the sample interval.

Acknowledgments

The authors are very pleased to acknowledge the dedicated scientists and engineers at Zygo Corporation who contributed to the success of the experiments, including J. Biegen, F. Demarest, A. Emars, C. Gaal, R. Gecewicz, K. Khalsa, C. Krajewski, W. Larson, T. Miles, R. Smythe and S. Uliasz.

References

[1] WYANT, J. C., 1993, *Laser Focus World*, September, 131.
[2] JOHONNOT, S., 1899, *Phil. Mag. Ser.* 5., **47,** 501.
[3] MICHELSON, A. A., 1893, *Astron. Astro-Phys.*, **12,** 556.
[4] BARNES, D. C., and PUTTOCK, M. J., 1953, *Engineer,* **196,** 763.
[5] FLOURNOY, P. A., MCCLURE, R. W., and WYNTJES, G., 1972, *Appl. Optics*, **11,** 1907.
[6] YOUNGQUIST, R. C., CARR, S., and DAVIES, D. E. N., 1987, *Optics Lett.*, **12,** 158.
[7] HITZENBERGER, C. K., 1992, *Appl. Optics*, **31,** 6637.
[8] FERCHER, A. F., MENGEDOHT, K., and WERNER, W., 1988, *Optics Lett.*, **13,** 186.
[9] HUANG, D., SWANSON, E. A., LIN, C. P., SCHUMAN, J. S., STINSON, W. G., CHANG, W., HEE, M. R., FLOTTE, T., GREGORY, K., PULIAFITO, C. A., and FUJIMOTO, J. G., 1991, *Science*, **254,** 1178.
[10] BALASUBRAMANIAN, N., 'Optical system for surface topography measurement', US Patent #4,340,306 (20 July 1982; filed 4 February 1980).

[11] DAVIDSON, M., KAUFMAN, K., and MAZOR, I., 1987, *Solid St. Technol.*, **30,** 57.
[12] LEE, B. S., and STRAND, T. C., 1990, *Appl. Optics*, **29,** 3784.
[13] DRESEL, T., HAEUSLER, G., and VENZKE, H., 1992, *Appl. Optics*, **31,** 919.
[14] KINO, G. S., and CHIM, S. S. C., 1990, *Appl. Optics.*, **29,** 3775.
[15] CHIM, S. S. C., and KINO, G. S., 1992, *Appl. Optics*, **31,** 2550.
[16] CABER, P. J., 1993, *Appl. Optics*, **32,** 3438.
[17] KOHLHASS, A., FROEMCHEN, C., and BRINKMEYER, E., 1991, *J. Lightwave Technol.*, **9,** 1493.
[18] DANIELSON, B. L., and BOISROBERT, C. Y., 1991, *Appl. Optics*, **30,** 2975.
[19] DE GROOT, P., 1992, *Optics Lett.*, **17,** 898.
[20] STEEL, W. H., 1983, *Interferometry*, 2nd edition (Cambridge: Cambridge University Press), pp. 256–257.
[21] DECK, L., and DE GROOT, P., 1993, *Proc. ASPE*, 424–426.
[22] DE GROOT, P., *Method and Apparatus for Surface Topography Measurement by Spatial-Frequency Analysis of Interferometry*, US patent pending. DECK, L., *Method and Apparatus for the Rapid Acquisition of Data in Coherence Scanning Interferometry*, US patent pending.
[23] BIEGEN, J., and SMYTHE, R., 1988, *Proc. SPIE*, 1009.
[24] DE GROOT, P., and DECK, L., 1993, *Optics Lett.*, **18,** 1462.
[25] KOHLHASS, A., FROEMCHEN, C., and BRINKMEYER, E., 1991, *J. Lightwave Technol.*, **9,** 1493.
[26] HARIHARAN, P., OREB, B. F., and EIJU, T., 1987, *Appl. Optics*, **26,** 2504.
[27] SANDOZ, P., and TRIBILLON, G., 1993, *J. mod. Optics*, **40,** 1691.
[28] MONTGOMERY, P. C., and FILARD, J.-P., 1992, *SPIE*, **1755,** 12.
[29] CABER, P. J., MARTINEK, S. J., and NIEMANN, R. J., 1993, *SPIE*, **2088,** 195.